LARGE DEPLOYABLE REFLECTORS: ENHANCING THE MESH REFLECTOR RF PERFORMANCES

L. Datashvili[(1)], N. Maghaldadze[(1)], M. Friemel[(1)], T. Luo[(1)], L. da Rocha-Schmidt[(1)], C. Cappellin[(2)], J. R de Lasson[(2)], R. Jørgensen[(2)], J.-C. Angevain[(3)], Alexander Ihle[(3)], Luca Salghetti Drioli[(3)]

[(1)] *Large Space Structures GmbH*
Hauptstr. 1e, 85386 Eching, Germany
Email: leri.datashvili@largespace.de

[(2)]*TICRA*
Landemærket 29, DK-1129 Copenhagen
Email: {cc,jrdl,rj}@ticra.com

[(3)]*ESTEC, Eurpean Space Agency*
Keplerlaan 1, Noordwijk, The Netherlands
Email: Jean.Christophe.Angevain@esa.int

ABSTRACT

Shaped surface reflector antennas are the preferred antenna type when a contoured beam illuminating a service region on the Earth from a communications satellite shall be achieved. The size of the reflector aperture (relative to the wavelength) determines the level of the minimum directivity on the service area and the directivity roll-off to areas using the same frequency and polarisation.

So far shaped surface reflector antennas have been usually manufactured with solid surfaces which ensures that the surface has the predicted shape. However, the aperture size is then limited by the available space and volume of the satellite configuration and launcher payload bay. A way to overcome this problem is to replace the solid reflector surface by a stowable and unfurlable mesh surface. Hence, the reflector in its stowed position during launch achieves a shaped (parabolic) reflecting surface once it is in its orbit. The challenges for this and some possible design solutions will be addressed in this paper both from an electrical as well as mechanical point of view for a shaping scenario of a large C-band reflector. Especially results achieved under the ESA project AMPER (Advanced Techniques for Mesh Reflector with Improved Radiation Pattern Performance) will be presented.

The investigation in RF performance carried out by TICRA covers the definition of several ranges of possible shaping with different shaping density. The mechanical and hardware implementation of the shaped surface is achieved by means of an equilibrium network carrying and properly tensioning the reflective metal mesh. Several LSS propriety analysis tools for proper form finding and optimization of the mesh type surfaces are used. This approach together with the iteration process between RF and mechanical analyses will be also presented.

In addition, different means of grating lobes reduction (GLR) of the large deployable mesh reflectors will be addressed via results achieved from RF investigations for finding the theoretical basis of a faceted surface arrangement. This will minimize the grating lobes to the acceptable levels.

Ongoing work is related to design and manufacturing of a shaped mesh reflector demonstrator of 2.3 m aperture diameter. The demonstrator will be tested in the planar near field scanner RF facility of ESA. Mechanical tests will also be carried out to support the applicability and verification of the prediction math models established.

1. INTRODUCTION

Some satellite applications are requiring a maximum antenna gain at a given angle. This requirement translates into the need of a pencil beam antenna where the peak gain is linearly depending on the antenna aperture. Other space applications are requiring the maximization of the minimum antenna gain over an arbitrary coverage defined by an angular sector. For such applications, the minimum gain is not linearly depending on the antenna aperture. It is well known that the figure of merit of gain-area product is bounded by a theoretical value of 41253 deg^2 assuming an antenna aperture of infinite size [1]. For an antenna aperture of finite size, a theoretical relationship between the figure of merit of the gain-area product and the circular antenna aperture can be derived [2]. This means that for high frequency applications such as the ones operating at Ku-band or Ka-band, the benefit of a large aperture for contoured beam antenna can be modest as compared to an antenna with moderate size. Therefore, in the context of producing a contoured beam, the interest of a large

unfurlable shaped reflector antenna cannot strictly be linked to the maximization of the minimum gain over a desired coverage only, but also on the minimization of the sidelobes that can be detrimental for some applications requiring an isolation gain, i.e. a sidelobe gain not to be exceeded over some service areas. This holds particular true for isolation areas that are in the vicinity of service areas, and that consequently require a steep gain slope. Large unfurlable shaped reflector antenna can therefore be a very interesting solution to meet stringent requirements regarding isolation gain or steep gain slope, in combination with minimum gain requirements that need to be met over a desired service area.

The interest of large shaped aperture to meet both wide scanning angle and stringent sidelobe requirements is also observed for multibeam application. Such application that are of paramount interest for telecommunication and Earth observation satellites require to produce multiple pencil beam with each beam pointing towards a single given angle. For these applications, the shaping of the reflector surface can be synthesized to produce a uniform peak gain for the multiple beam over the angular area of interest [3] [4]. Such technique allows to minimize the scan loss over this area. This synthesis technique for reflector shaping can also be used to minimize the sidelobes of each beam [5], and can be combined with the scan loss minimization technique.

Lastly, the faceting error that is peculiar to the current design of metallic mesh reflectors translates into the presence of grating lobes in the radiation pattern of the unfurlable antenna. This is due to the phase error, also called the RF path length error, occurring between the mesh reflector surface consisting of a regular arrangement of quasi-flat triangular facets and the ideal smooth paraboloidal surface of the reflector. A further condition for the presence of the grating lobes is that the size of the facets, that are regularly and repeatedly arranged over the reflector surface, exceeds the wavelength of operation. The presence of high grating lobes can have a negative impact for some applications. It can be the case of radiometric application where the grating lobes are coincidently observing undesired areas with high brightness temperature that can either be of natural origin such as the sun or of artificial origin such as local RF interferers. Such occurrence may pollute the radiometric observation measurements where a high accuracy is very often required. It can therefore be of interest to find design techniques to minimize the level of the grating lobes, that are inherent to the design of mesh reflectors.

2. GRATING LOBE REDUCTION TECHNIQUES

We consider here a single offset reflector with projected aperture diameter of D = 12 m, normalized focal length of f/D = 0.7 and a clearance of d' = 1.5 m. We focus on L band and a frequency of 1.4 GHz, and for the feed we use a linearly polarized Gaussian with a feed taper at the reflector edge of -12 dB.

2.1. Origin of grating lobes

Faceting of the mesh reflector surface with facet nodes sitting exactly on the nominal smooth parabolic surface and with nodes connected by *planar* triangles produces a surface error between the nominal and the mesh reflector surface. The simplest approach for positioning nodes is in a uniform hexagonal mesh, implying that the triangles forming the mesh are equilateral with the side length s being the only parameter.

Figure 1 displays a nominal smooth parabolic surface (left) and a uniform hexagonal mesh reflector surface (right). The surface difference (Δz) between the two surfaces is shown in the central panel. Bright spots are the nodes, placed exactly on the nominal surface, whereas dark regions correspond to the abovementioned planar triangles.
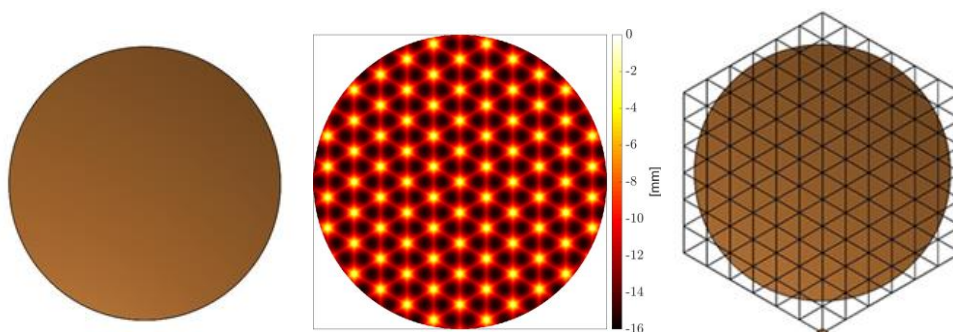

Fig. 1. Left: Nominal smooth parabolic surface. Center: Surface difference (Δz) between nominal and mesh reflector surface. Right: Uniform hexagonal mesh reflector surface.

In Fig. 2, we display the co-polar patterns for both reflector surfaces, and in the left panel we observe the characteristic pencil beam of the nominal surface, with a distinct maximum and sidelobes. For the mesh surface (right panel), we also observe a maximum and sidelobes, but in addition undesirable grating lobes; these are a direct consequence of the *periodic* surface error.
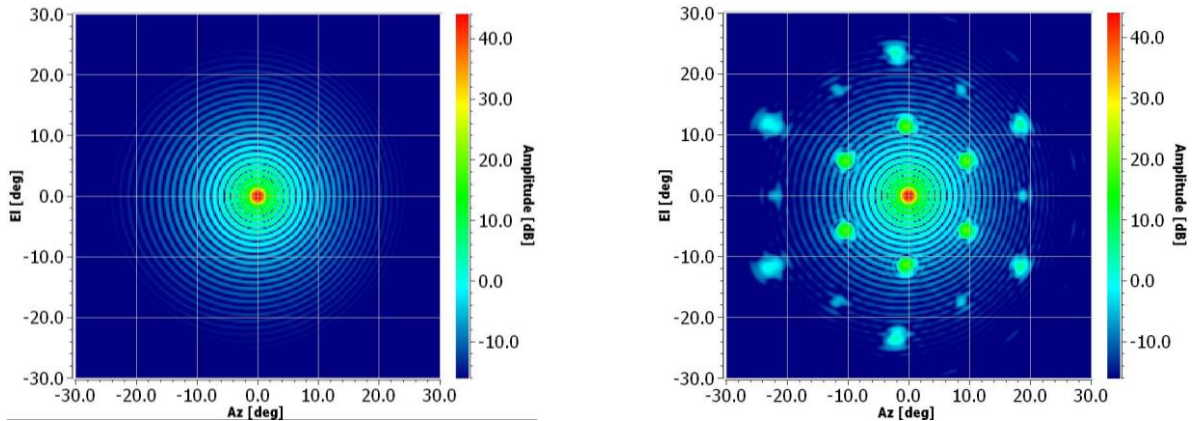

Fig. 2. Co-polar far-field patterns for reflector surfaces in Fig. 1. Left: Nominal smooth parabolic surface. Right: Uniform hexagonal mesh reflector surface.

2.2. Reducing grating lobes with non-uniform meshes

In the limit of the uniform mesh triangle side length *s* going to zero, we recover the nominal paraboloid and the grating lobes vanish. Therefore, one approach for reducing the grating lobes is to reduce the side length until the grating lobes have been sufficiently suppressed. This is straightforward in RF computations, but as the side length is decreased, more nodes are required to form the mesh, which increases the mechanical complexity of the reflector.

An alternative approach, that we have followed, is to maintain the same *average* side length in the mesh, but to break the periodicity to reduce the grating lobes, that is, to consider non-uniform mesh configurations [6]-[9]. In an initial part of the study, we investigated a number of the configurations previously proposed in the literature [10], which led to the conclusion that the so-called arithmetic mesh [6] appeared most promising for grating lobe reduction. An example of the arithmetic mesh is shown in the left panel in Fig. 3. It looks similar to the uniform mesh, but the side lengths are "stretched" from the center and outwards, so that triangles are smaller in the center and larger towards the reflector edge. This mesh as well as all other non-uniform meshes all exhibit a surface error compared to the nominal paraboloid, but the surface error is not periodic as for the uniform mesh (see Fig. 1). The arithmetic mesh exhibits a six-fold symmetry, while an alternative is to change the mesh to exhibit a five-fold symmetry [7]; such a pentagonal arithmetic mesh is shown in the right panel in Fig 3. To further improve the mesh reflector patterns, in particular to lower the first sidelobe [6], [10], we finally allowed the feed to move away from the position that is ideal for the nominal paraboloid. Specifically, we introduced manual shifts of position and orientation of the feed, and we also optimized its position and orientation using the POS software [11]. The best result, as summarized in the following section, was obtained by shifting the feed closer to the reflector along its own axis; this shift gives rise to a more uniform phase of the reflected field [7], which leads to a lower first sidelobe, while still maintaining a significant grating lobe reduction.
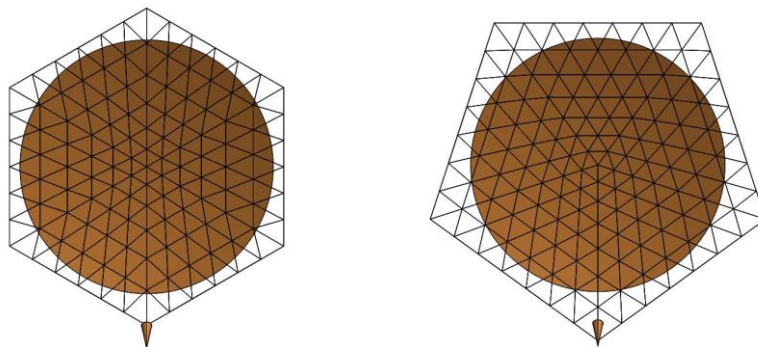

Fig. 3. Arithmetic meshes. Left: Hexagonal. Right: Pentagonal.

2.3. Results for grating lobes reduction

To quantify the ability of different configurations to reduce grating lobes, we look at the pattern grid difference between the given mesh reflector and the nominal paraboloid envelope grid; such grids exhibit maxima at the positions of the grating lobes [10]. This quantity is collected for different types of surfaces in the second column in Table 1, while the third column collects the increase of the first sidelobe (maximum from E- and H-planes) compared to the nominal paraboloid.

Table 1. Grating lobe strength and maximum increase of first sidelobe level for different surfaces.

Surface	Grating Lobe Strength [dB]	Max[ΔFirst Sidelobe] [dB]
Nominal	0	0
Uniform hexagonal	23.88	0.88
Arithmetic, hexagonal	15.99	4.26
Arithmetic, pentagonal	14.23	3.95
Arithmetic, pentagonal, feed shifted 100 mm	14.85	0.23
LSS network, force equilibrium	15.33	1.09

The uniform hexagonal gives rise to grating lobes with pattern values that are 23.88 dB above the pattern level of the nominal surface. Going to the non-uniform arithmetic surfaces decreases this value to 15.99 dB and 14.23 dB for the hexagonal and pentagonal meshes, respectively. However, these meshes give a first sidelobe that is about 4 dB larger than for the nominal paraboloid. Shifting the feed 100 mm closer to the reflector along its own axis, slightly degrades the grating lobe reduction (by 0.6 dB), but also brings the first sidelobe down to the level of the nominal paraboloid.

The meshes considered this far are theoretical RF meshes that are not in mechanical equilibrium. Inspired by the pentagonal arithmetic mesh, we have generated a network with nodes in mechanical equilibrium (Figure 4) and analysed its RF performance in GRASP; the numbers are collected in the last line in Table 1. It has a grating lobe reduction of approximately 8.5 dB compared to the uniform hexagonal mesh.
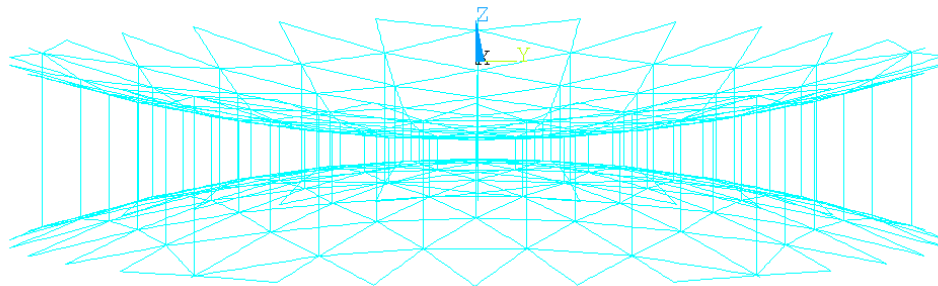

Fig. 4. Optimized mechanical design of the cable network for GLR, side view

Mechanical investigations and analysis have been performed on the facet distribution cases suitable for manufacturing. For example, Fibonacci mesh, bipolar mesh and Penrose mesh have been refused from the point of manufacturing complexity. On the other hand, arithmetic meshes gave better configurations i.e. as shown in the Figure 4.

Owning this technique of mechanical design and development of the cable networks for GLR, a demonstrator of such reflector is being built for Ka-band frequency within the same project. As a reflecting mesh, a knitted metal mesh from Tec-Knit, Germany, will be used. The reflector is targeting small satellite applications, including CubeSats, although it follows highly scalable architectures of LSS reflectors [13] - [15] and is suitable for large diameters up and above 18 m.

3. MESH REFLECTOR SHAPING

Shaped surface reflector antennas is the preferred antenna type when a contoured beam illuminating a service region on the Earth from a communications satellite shall be implemented.

The size of the reflector aperture (relative to the wavelength) determines the level of the minimum directivity on the service area and the directivity roll-off to areas using same frequency and polarisation.

So far shaped surface reflector antennas have been manufactured with solid surfaces which ensures that the surface has the predicted shape. However, the aperture size is then limited by the volume of the space bus.

A way to overcome this problem is to replace the solid reflector surface by an unfurlable mesh surface. Hence, the reflector is in stowed position during launch and once in orbit it is deployed. The advantage/drawback of this solution compared to traditional solid surface shaping is the subject of this study.

3.1. Input data

In this study it has been decided to use an INTELSAT-10 C-band mission as model for assessing the capability of the mesh surface in shaped surface reflector antennas. In Fig. 5 the service areas are shown. The North-East (NE) area has a central high-gain area in which the level is forced to be 4 dB higher than in the rest of "North-East". The level on NE is maximized and simultaneously the level on West-Hemi (WH) is minimized.

Furthermore, Fig. 5 shows the antenna geometry which shall provide this illumination. It is an offset single reflector geometry of which the starting point is a paraboloidal reflector.
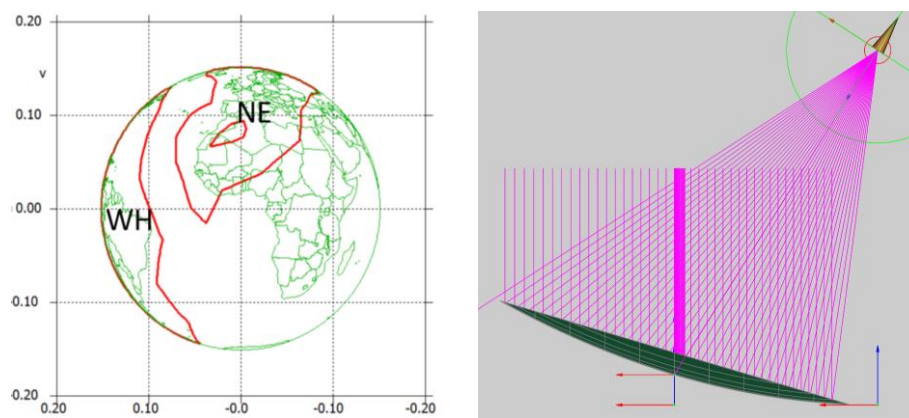

Fig. 5   INTELSAT-10 service area scenario (left) and side view of initial reflector geometry before shaping.

The geometrical parameters are the following:

- Frequency 3.625 GHz, 4.2 GHz, 5.85 GHz and 6.425 GHz
- Main reflector diameter 6 m
- Focal length 6 m
- Main reflector offset (from paraboloid axis to aperture centre) 3.5 m
- Main reflector offset angle 30.83°.
- Main reflector half-cone angle 25.95°.
- Hybrid-mode feed horn - aperture diameter 228 mm
- Antenna West wall mounted on satellite - pointing towards the sub satellite point.

3.2. Surface shaping

By means of the POS software the reflector surface is now shaped by adding to the initial paraboloid a delta surface which is constructed from a set of spline coefficients defined in a grid in the reflector aperture. A shaping with slowly varying ripple (16-by-16 grid points) and quickly varying ripple (32-by-32 grid points) has been done. The quickly varying ripple has the advantage that a higher field level in the "North-East" zone can be obtained. On the other hand, it can be more difficult to reproduce with facets.

After optimisation of these splines the surface profile and the field distribution look as shown in Fig. 6. The level in the central high-gain zone of "North-East" is 4 dB higher than in the remaining part of "North-East".
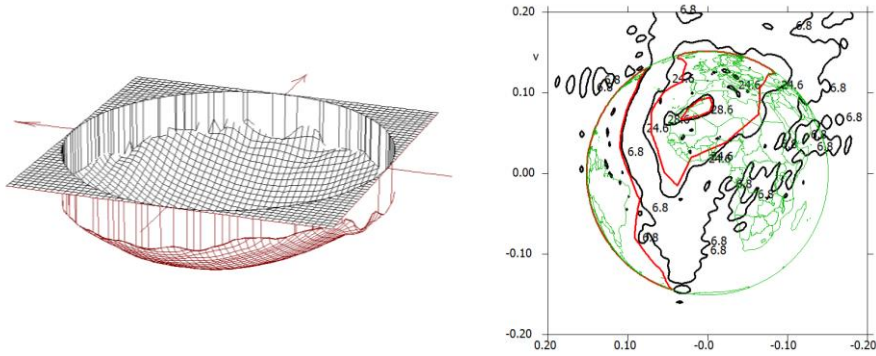
Fig. 6   3D-view of surface shaping (delta surface for 16-by-16 splines) and optimized contoured beam on INTELSAT-10 NE area. Minimum level on NE high/low is 28.6/24.6 dBi. Maximum level on WH 6.8. dBi. Field shown at 3.625 GHz

3.3   Analysis using optimized facetted surfaces

According to the surface profiles found by the POS surface shaping (an example is shown in Fig. 6), respective optimized cable networks have been designed for the 16-by-16 spline case and the 32-by-32 spline case. Mesh lay-out using 6 different facet side length values have been analysed.
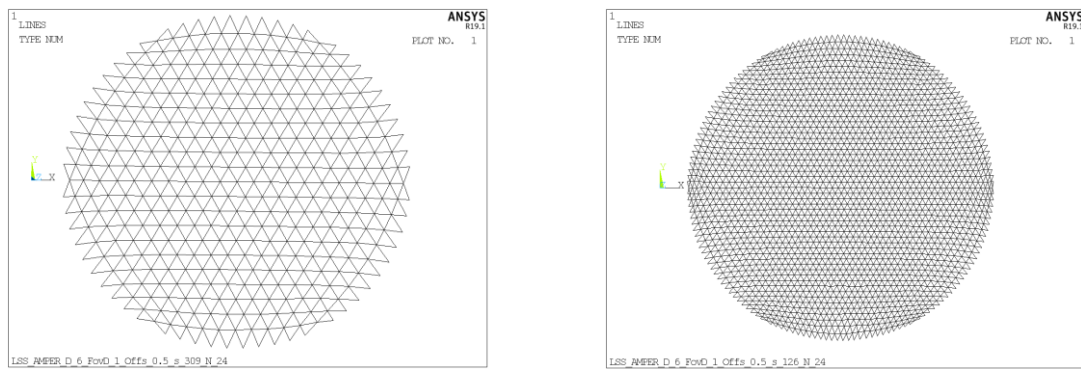

Fig. 7 Cable Network lay-out for facet length 309 mm (maximum) and 126 mm (minimum)

In Fig. 7, two design examples are shown with two different facet side length. Side length values of 162 mm, 200 mm, 243 mm and 284 mm have also been included in the analysis. Facet length determines the number of facet rings on the reflecting surface, which is defined as a variable for the shaped networks optimization and form finding.

In each node point the coordinate fits exactly the coordinate of the input smooth surface found by the POS optimization. In each facet the surface is planar. With small facet side length the analysed minimum field level values will be close to the values obtained with the smooth surface. On the other hand, the mechanical setup is more complicated as more points have to be kept in position with cables.

Table 2 Comparison of optimization result in POS with analysis when smooth surface is replaced by facetted surface. The 3 dBi values for each frequency are "North East low", "North East high" and "West Hemi".

	Smooth surface	Facet topologies with side length, [dBi]				
Freq.	POS opt. [dBi]	162 mm	200 mm	243 mm	284 mm	309 mm
	24.6	24.1	23.8	23.5	23.3	23.2
3.625 GHz	28.6	28.2	28.0	27.7	27.3	27.1
	6.8	9.2	9.8	10.8	11.4	11.7
	24.6	24.4	24.3	24.2	24.3	24.3
4.200 GHz	28.6	28.6	28.6	28.6	28.7	28.8
	6.8	8.7	9.4	10.0	8.8	8.4
	24.6	24.6	24.6	24.4	24.2	24.0

5.850 GHz	28.6	28.6	28.7	28.9	29.0	29.0
	6.8	8.5	8.6	8.2	7.9	7.6
	24.6	24.2	24.1	23.9	23.6	23.5
6.425 GHz	29.1	29.1	29.1	29.0	29.1	29.2
	6.8	7.5	8.4	9.1 di	9.3	8.5

In Table 2 it is obvious to see that applying the smallest facet side length (162 mm) the analysed values are close to the values optimised for the smooth surface ("West hemi" is slightly higher). For the largest side length (309 mm) the degradation is significant.

3.3. Investigations on accuracy of the shaped networks of mesh surfaces

Four target shapes have been developed with and without applied curvature limitations and different parameter variations. These four shapes are numbered as case 4, 6, 8 and 9 below in the text. Investigations of the networks' shaping targeting the four shapes has been performed aiming finding the influence of those parameters on the final shape accuracy.

Variation of number of facet rings, which is a highly influencing parameter, has been applied as well. This parameter was varied between 7 and 24 that give networks still possible to manufacture with more or less complexities. Examples of the designed RF reflective networks with about 2.5 m diameter aperture are given below in Figure 8 with 7, 16 and 24 facet rings.
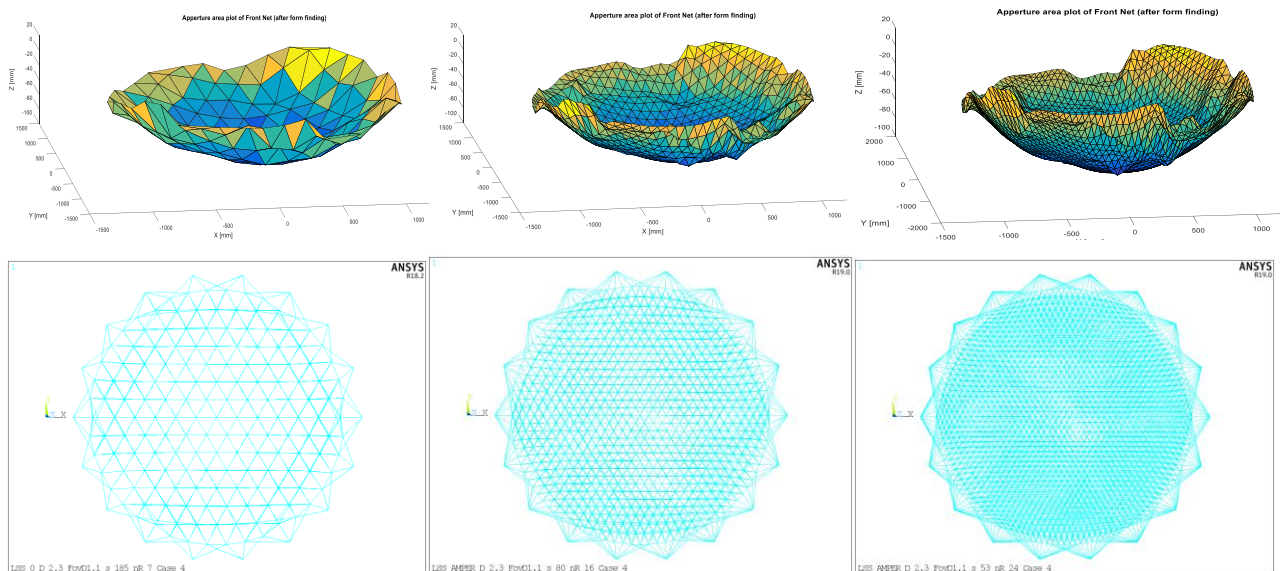

Fig. 8 Cable Network lay-out for facet length 185 mm (left), 80 (middle) and 52 mm (right), in iso- and top views

In Figure 8 cable networks are shown, which have been designed targeting the same shaped surface. The higher the number of surface divisions, the better matching resulted.

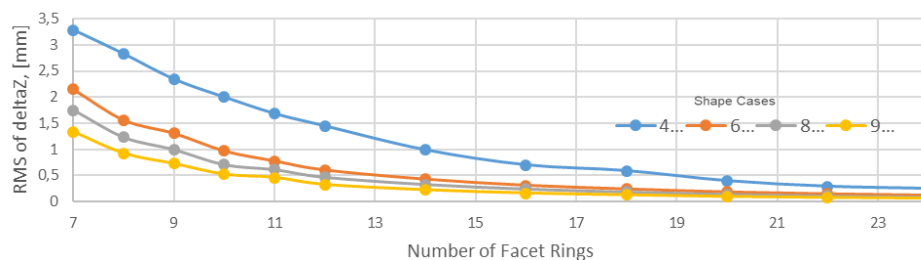RMS accuracies for each of the analysed shape and network cases are depicted in Figure 8.

Fig. 9 RMS accuracy of the shaped faceted surfaces vs. the target shapes

It can be observed from the figure that, the higher the number of facets the better RMS is achieved. In the same way, as expected, the higher curvature radius limit was set, the better RMS is resulted with less facets.

Generally, shaping of the RF surfaces requires very high curvature regions, which are then approximated by facets. The facets then get located with larger angels to each other (as compared to the parabolically shaped networks). Due to this reason pillowing effect appears significant. To assess the mesh surface accuracy and compare to the flat faceted surface, a pillowing accuracy analysis has been carried out. Results are plotted in Fig. 10 showing the differences.
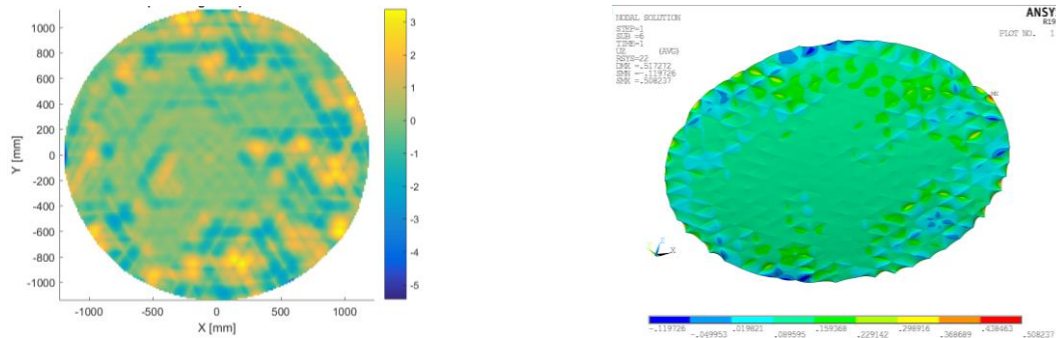

Fig. 10 Plots of shape differences: target shape vs. faceted shape (left), pillowed shape vs. faceted shape (right)

Shape of the mesh reflecting surface, which is under prestress with the faceted network, gets pillowed losing about 25% of the accuracy as compared to the ideal facets vs. target shape. This value depends on the prestress levels in the whole RF surface assembly and optimization of RF performances considering this effect shall be carried out for the good design.

3.4. Design of the shaped RF surface assembly demonstrator and its test setup

A 2.5 m shaped RF surface assembly demonstrator has been designed and is being built. Shape accuracy test and RF tests will be carried out, as well as other mechanical tests, all for validating the structural FEM and RF models. The network design of the RF surface assembly is selected according to one of the investigated cases and the accuracy and RF performance will be compared to the predictions. The RF test setup of the RF surface assembly is shown in Fig. 11.
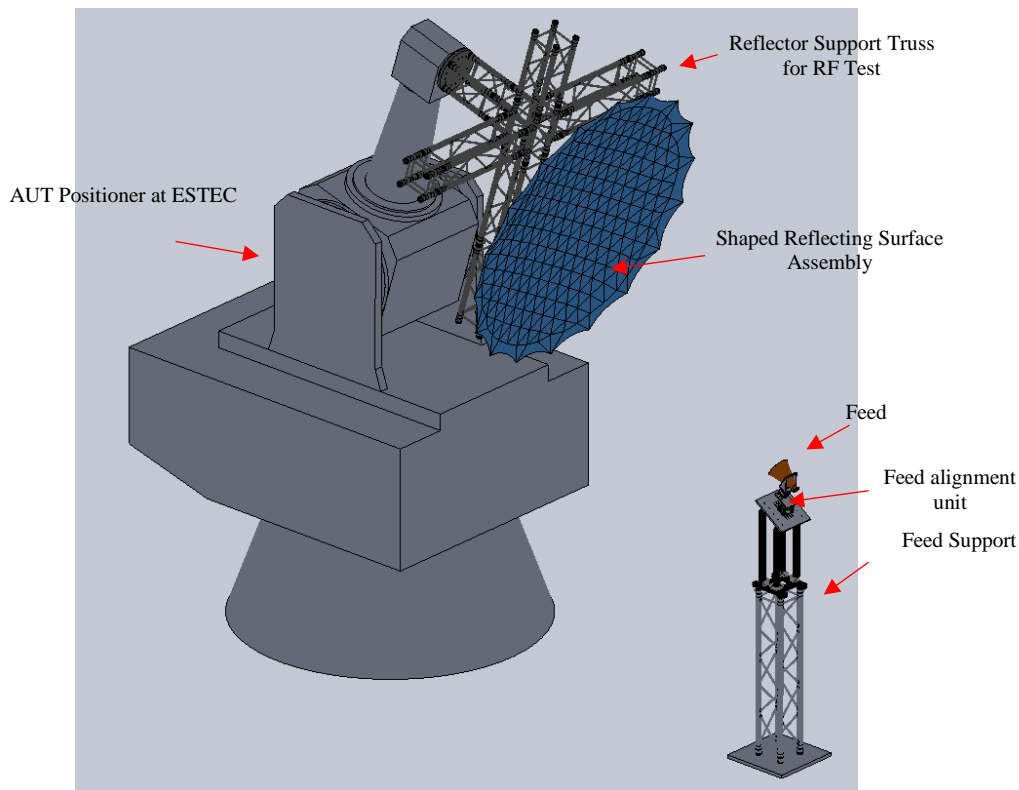

Fig. 11 Plots of shape differences: target shape vs. faceted shape (left), pillowed shape vs. faceted shape (right)

The RF surface assembly, consisting of the metal knitted mesh and supporting cable network, is tensioned using a stiff ring (not shown in the figure), which is mounted on the support truss. The reflector support truss is mounted on the interface of the roll of the ESTEC/ESA facility positioner system. The feed with its precise positioning and alignment system is on a standalone support truss tower. As a reflecting surface, metal knitted mesh made of gold plated tungsten wire will be used. It is manufactured by HPS, Germany. RF measurements will be performed in C-band. Other higher frequencies are also under consideration.

The RF surface assembly was modelled in ANSYS FEM software with all the support structure and gravity compensation system. The FEM analysis is performed to investigate the RF surface deformation under the gravity load during the RF test in the same position and orientation as during the tests. The gravity load is applied in the corresponding direction to simulate the RF test setup condition.

The out-of-plane deformations of the RF faceted surface are plotted in Fig. 12 in mm units. It shows that the rigid body rotation contributes to the major part of the RF surface deformation due to inclined orientation of the reflector. This will be corrected by the positioner and alignment unit. The actual deformations of the surface are rather small. The Surface best-fitting and the RMS calculation are performed to characterize the deformations.

The out-of-plane shape difference between the deformed facets (gravity load) and the initial shape of the surface is shown in Figure 3. The best-fit RMS of gravity deformations equates to 0.0346 mm.
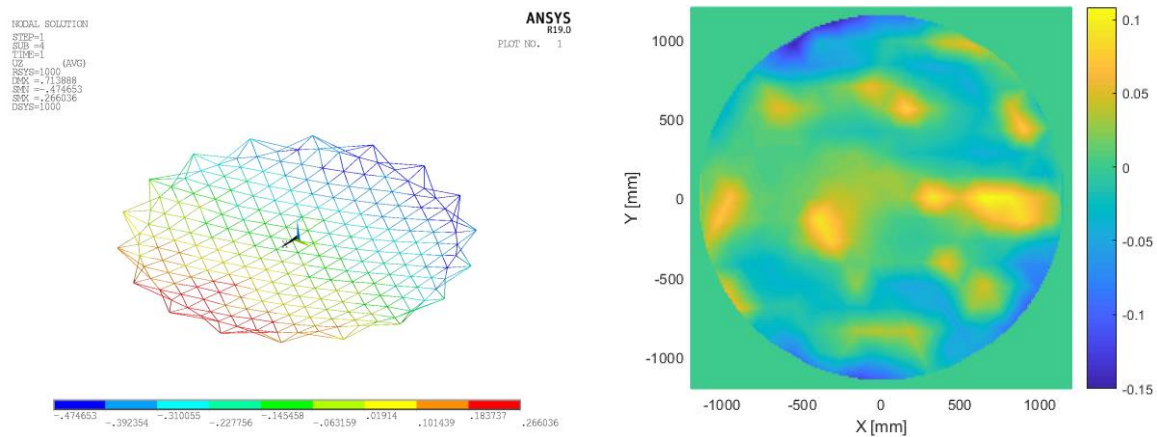

Fig. 12 The out-of-plane deformation of the shaped cable network under the gravity load

The relative translations and rotations of the best-fit RF surface are listed in Table 3 in the aperture coordinate system. The major changes are the translations and the elevation. These translations and rotations, as mentioned, can be well compensated by the AUT positioner system and the feed precise alignment system.

Table 3: The relative translations and rotations of the best-fit surface

X translation	-0.582 mm
Y translation	0.002 mm
Z translation	-0.107 mm
X rotation	0.0007°
Y rotation	0.0180°
Z rotation	-0.0008°

It is remarkable, that such a precise design of the RF surface assembly combined with the precise accuracy and RF measurements shall allow high level of validation of the simulation models for both, structural as well as RF models.

4. CONCLUSIONS

Results of extensive investigations of in two tasks have been given in this paper: for large reflectors shaping and for grating lobes reduction, both to result into the improved RF performance of the large deployable mesh reflectors.

Iterative approach was applied between the RF and mechanical analysis by TICRA and LSS respectively. In both tasks, significant achievements shall be highlighted:

Shaping: a coverage was targeted, which resulted into complex shapes for mechanical implementation. Nevertheless, certain improvements of performances (e.g. isolation) have been achieved whereas the minimum gain over coverage has been degraded as compared to the existing conventional shaped solid reflectors of 3-meter diameter size. For some other simpler shapes, fulfillment of requirements has been assessed and demonstrated.

GLR: investigations in GLR resulted into a solution which gives full satisfaction of requirements: reduction of grating lobes of 8.55 dBi is achieved while the requirement was to reduce at least 7 dBi.

Two reflector demonstrators are under constructions at LSS for demonstrating achievements of the both tasks discussed: 1.2 m Ka-band reflector for GLR targeting small satellite applications, including CubeSats, and scaled 2.6 m C-band reflector for applications in shaped surface LDRs up to 8 m and beyond.

ACKNOWLEDGEMENTS

REFERENCES

[1] J.D. Thompson, "Flat-topped antenna beams with maximum gain-area product", 2007 IEEE Antennas and Propagation Society International Symposium (APS2007), 9-15 June 2007, Honolulu, Hawai, USA.

[2] H. Luh, "Gain-area product of circular aperture", IEEE Transactions on Antennas and Propagation, Vol.36, Issue 8, August 1988

[3] N. Albertsen, K.Pontoppidan, S. Sorensen,"Shaping of dual reflector antennas for improvement of scan performance", 1985 IEEE Antennas and Propagation Society International Symposium, 17-21 June 1985, Vancouver, Canada

[4] W.P. Craig, C.M. Rappaport, J.S. Mason,"A high aperture efficiency, wide-angle scanning offset reflector antenna", IEEE Transactions on Antennas and Propagation, Vol.41, Issue 11, November 1993

[5] Y. Demers, E.Amyotte, K. Glatre, M.-A. Godin, J. Hill, A. Liang, M. Riel,"Ka-band User Antennas for VHTS GEO Applications", 11th European Conference on Antennas and Propagation (EuCAP2017), 19-24 March 2017, Paris, France

[6] T. Orikasa, T. Ebisui, and T. Okamoto, "Sidelobe suppression of mesh reflector antenna by non-regular intervals," in Antennas and Propagation Society International Symposium. AP-S., June 1993, pp. 800–803.

[7] A. C. Brown, "Irregular segmentation of paraboloidal reflectors," in Antennas and Propagation Society International Symposium. AP-S., July 1996, pp. 242–245.

[8] Y. Zong, B. Duan, Y. Ban, W. Wang, W. Xu, C. Wang, J.Du, "Surface configuration design of cable-network reflectors considering the radiation pattern", IEEE Transactions on Antennas and Propagation, Vol.62, No.6, June 2014.

[9] J.C. Angevain, G. Rodrigues, J. Santiago-Prowald, C. Mangenot, L. Datashvili, "Sidelobe level reduction of faceted mesh reflector antenna using phyllotactic arrangements", 2nd International Scientific Conference Advanced Lightweight Structures and Reflector Antennas, 1-3 October 2014, Tbilisi, Georgia.

[10] C. Cappellin, J. R. de Lasson, R. Jørgensen, L. Datashvili, J. Pauw, N. Maghaldadze, M. Migliorelli, and J. C. Angevain, "Large mesh reflectors with improved pattern performances," in 37th ESA Antenna Workshop, November 2016.

[11] POS Software, TICRA, Copenhagen, Denmark, www.ticra.com.

[12] J. R. de Lasson, C. Cappellin, R. Jørgensen, L. Datashvili, and J. C. Angevain, "Advanced Techniques for Grating Lobe Reduction for Large Deployable Mesh Reflector Antennas," in Antennas and Propagation Society International Symposium. AP-S., July 2017, pp. 993-994.

[13] Datashvili L.; Maghaldadze N.; Baier H.; Friemel M.; da Rocha-Schmidt L., "High TRL Achieved for European Large Deployable Reflector Antennas", proceedings of EuCAP 2018, London, UK, 2018

[14] L. Datashvili, "Deployable Space Reflector", Georgian Patent #GE P 2017 6727 B, 2012 Oct. 19

[15] Datashvili, L.: "Foldability of hinged-rod systems applicable to deployable space structures", CEAS Space Journal (5), 2013, S. 157 – 168